

Observed cosmic evolution of galaxy dust properties with metallicity and tensions with models

Gergö Popping^{1*} & Céline Péroux^{1,2}

¹European Southern Observatory, Karl-Schwarzschild-Str. 2, D-85748, Garching, Germany

²Aix Marseille Université, CNRS, LAM (Laboratoire d'Astrophysique de Marseille) UMR 7326, 13388, Marseille, France

Accepted XXX. Received YYY; in original form ZZZ

ABSTRACT

The dust abundance of the interstellar medium plays an important role in galaxy physics, the chemical evolution of matter and the absorption and re-emission of stellar light. The last years have seen a surge in observational and theoretical studies constraining the dust-abundance of galaxies up to $z \sim 5$. In this work we gather the latest observational measurements (with a focus on absorption studies covering metallicities in the range $6.8 < 12 + \log(O/H) < 9$) and theoretical predictions (from six different galaxy formation models) for the dust-to-gas (DTG) and dust-to-metal (DTM) ratio of galaxies. The observed trend between DTG and DTM and gas-phase metallicity can be described by a linear relation and shows no evolution from $0 < z < 5$. Importantly, the fit to the DTG-metallicity relation provides a refined tool for robust dust-based gas mass estimates inferred from millimeter dust-continuum observations. The lack of evolution in the observed relations are indicative of a quickly reached balance (already when the Universe was 1.2 Gyr old) between the formation and destruction of dust and a constant timescale for star-formation at fixed metallicities over cosmic time. None of the models is able to reproduce the observed trends over the entire range in metallicity and redshift probed. The comparison between models and simulations furthermore rules out some of the current implementations for the growth and destruction of dust in galaxy formation models and places tight constraints on the predicted timescale for star-formation.

Key words: galaxies: formation – galaxies: evolution – galaxies: ISM – ISM: dust, extinction – methods: numerical

1 INTRODUCTION

A fundamental component of galaxy formation is the cycle of baryons in and out of galaxies. This picture emerges from both simulations and observations alike (Péroux & Howk 2020; Walter et al. 2020). The flow of gas, metals, and dust between stars, the interstellar medium, and circum-galactic medium has a tremendous impact on galaxy evolution. The transfer of metals between interstellar gas and the dust phase, in particular, constitutes an important component of this baryon cycle.

Interstellar dust is known to be made of small solid particles (grains distributed in size with an average of $\sim 1 \mu\text{m}$) of carbon, silicates, and ices from other chemical species (Draine 2003). Despite the small mass fraction in dust (1%) compared to gas in the interstellar medium of galaxies (99%, e.g., Rémy-Ruyer et al. 2014), dust has a tremendous impact in several fundamental physical processes. Dust plays a key role in the radiative transfer, chemistry, and thermodynamics which all profoundly impact galaxy evolution. In addition, a substantial fraction of all the metals produced in the Universe are locked into solid-phase dust grains (approximately 44 per cent for the Milky Way, based on Rémy-Ruyer et al. 2014).

Dust is critical in the thermal balance of gas as well as in shielding

the cores of dense clouds from ultra-violet radiation, allowing for the formation of molecules which are critical to the star-formation process. The surfaces of dust grains catalyse a range of chemical reactions that influence the structure of interstellar medium and star formation (Hollenbach & Salpeter 1971; Hollenbach et al. 2012; Gong et al. 2017). In addition, they are responsible for the heating of the gas in photodissociation regions by the photoelectric effect (Draine 1978). These effects have poorly constrained efficiencies and are highly environment dependent due to radiative transfer effects. Dust also acts as an efficient catalyst of the formation of the most abundant molecule in the Universe, molecular hydrogen (H_2) in the interstellar medium (e.g., Gould & Salpeter 1963; Cazaux & Spaans 2009; Romano et al. 2022). Indeed, giant molecular clouds composed of molecular gas are the major formation sites of stars in galaxies (e.g., Blitz 1993; Fukui & Kawamura 2010). In turn, dust absorption of far-ultraviolet and optical photons can shape the temperature structure of the neutral interstellar medium (Goldsmith 2001; Krumholz et al. 2011; Liang et al. 2019).

Dust grains also play a crucial role in radiative processes within the interstellar medium by absorbing ultraviolet and optical starlight and reradiating it at far-infrared wavelengths. An important observational consequence of this property is a induced change in the spectral energy distributions of galaxies (Calzetti et al. 2000; Buat et al. 2002; Salim & Narayanan 2020). As a consequence, our census of the star-

* E-mail: popping@eso.org

formation rate (SFR) density of the Universe with cosmic time is highly incomplete unless we include the fraction of star formation obscured by dust (e.g., Steidel et al. 1999; Takeuchi et al. 2010; Kennicutt & Evans 2012; Madau & Dickinson 2014; Bouwens et al. 2020; Gruppioni et al. 2020; Fudamoto et al. 2021).

Dust furthermore has an impact on gas dynamics in dusty clouds through radiation pressure (e.g., Ishiki & Okamoto 2017). Moreover, the typical mass of the final fragments in star-forming clouds is regulated by dust cooling (Whitworth et al. 1998; Omukai 2000; Omukai et al. 2005; Larson 2005; Schneider et al. 2006) with potential dramatic impact on the stellar initial mass function. For example, recent theoretical work suggests that the initial mass function in metal-poor (and dust-poor, $Z/Z_{\odot} \approx 10^{-5}$) environments is top heavy compared to a Chabrier (Chabrier 2003) initial mass function (Chon et al. 2021).

The ejection of dust from galaxies contributes to the metal enrichment of the circumgalactic and ultimately intergalactic medium while providing an additional cooling channel (Ostriker & Silk 1973; Ménard et al. 2010; Peebles et al. 2014; Peek et al. 2015; Vogelsberger et al. 2019; Péroux et al. 2020; Wendt et al. 2021). Eventually, dust coagulation in proto-planetary discs becomes a key ingredient of planet formation (e.g., Okuzumi et al. 2009; Kataoka et al. 2014).

For all these reasons, a complete diagnostic of dust physical characteristics and their relation to galaxy properties are essential. Establishing the galactic scaling relationships that apply to dust thus appears a natural tool. Specifically, the dust-to-gas ratio (hereafter DTG) quantifies the fraction of the interstellar mass locked onto dust grains. It is defined as the dust mass divided by the gas mass or alternatively dust surface density (or column density) divided by the gas surface density (or column density). Likewise, the dust-to-metals ratio (DTM) represents the fraction of the metal mass incorporated into the solid phase. The DTG and DTM ratios are fundamental parameters resulting from the interstellar gas-dust cycle, and are expected to substantially vary with environment and in particular gas metallicity (Lisenfeld & Ferrara 1998; Draine & Li 2007; Galliano et al. 2008). The relation between the DTG and DTM of galaxies as a function of their metallicity provides key constraints for the physics and timescales governing the buildup and destruction of dust in galaxies (e.g., Asano et al. 2013; Rémy-Ruyer et al. 2014; Zhukovska 2014; Feldmann 2015).

The goal of this work is to provide a new appraisal of the dust abundance in galaxies as a function of both galaxy properties and cosmic time with the aim to assess their impact on our current knowledge of galaxy evolution. To this end, we have gathered the latest observational measurements and results from a selected sample of state-of-art semi-analytical and hydrodynamical simulations. A broad comparison between observations and simulations is very timely, as in the last five years significant advancements have been made in constraining the DTG and DTM of galaxies at $z > 0$ through absorption and emission studies (De Cia et al. 2016; Wiseman et al. 2017; Péroux & Howk 2020; Shapley et al. 2020) and modeling these properties in cosmological simulations (e.g., Mancini et al. 2015; Popping et al. 2017; Ginolfi et al. 2018; McKinnon et al. 2018; Li et al. 2019; Triani et al. 2020; Vijayan et al. 2019; Hou et al. 2019; Graziani et al. 2020; Kannan et al. 2021; ?).

This paper is organised as follows. In Section 2 and Section 3 we present the observations and simulations used in this work, respectively. The comparison between the two is presented in Section 4, whereas we discuss and summarise the results in Sections 5 and 6. We adopt the following cosmological parameters (Planck Collaboration et al. 2016): $H_0 = 67.74 \text{ km s}^{-1} \text{ Mpc}^{-1}$, $\Omega_M = 0.3089$, and $\Omega_{\Lambda} = 0.6911$.

Table 1. Linear regression fits to the observed DTG and DTM evolution with metallicity plotted on Fig 1. Note that the DTM and DTG are correlated such that $\text{DTM} = \text{DTG} / Z$, where Z is the gas-phase metallicity expressed as $M_{\text{metal}} / M_{\text{gas}}$.

	Redshift	Slope	Intercept	Reference
log DTG	$z=0$	2.45	-23.30	De Vis et al. (2019)
	$z>0$	1.30	-13.72	this work
log DTM	$z>0$	0.32	-3.28	this work

2 OBSERVATIONAL COMPILATION

In this Section we present the data compilation used in this work to explore the relation between DTG and DTM of galaxies with metallicity and their cosmic evolution. We first discuss the compilation of local galaxies with DTG and DTM information based on their emission (Section 2.1) and then discuss the $z > 0$ compilation based on absorption measurements (Section 2.2).

2.1 Local Measurements of DTG & DTM

The DTG and DTM values are well constrained in our Galaxy, based on modeling the infrared emission and optical/ultraviolet extinction (e.g., Draine & Li 2007). Modern surveys provide fresh measurements of these quantities in galaxies beyond the Milky Way (Lianou et al. 2019; Vílchez et al. 2019). A remarkable coordinated effort undertaken under the DustPedia collaboration has assembled observational constraints on DTG and DTM from a large sample of nearby galaxies (e.g., Rémy-Ruyer et al. 2014; De Vis et al. 2019; Galliano et al. 2021). In this work, the dust masses are estimated from a Spectral Energy Distribution (SED) fit to the galaxy photometry. The total gas mass is the sum of direct HI-emission mass measurements and H_2 masses estimated through CO observations (Rémy-Ruyer et al. 2014) or estimated assuming H_2 -to-HI and HI-to-stellar mass ratios (De Vis et al. 2019). The gas-phase oxygen abundances are derived using multiple strong emission-line calibrations (using the Pilyugin & Grebel 2016 S-calibration, based on N_2 , R_2 and S_2). We note that metallicities based on strong emission-line calibrations have been reported to present significant dispersion depending on the calibration used (up to 0.3–0.4 dex Kewley & Ellison 2008; Scudder et al. 2021). All these quantities are integrated over the whole galaxy. The resulting data are reproduced in the left panels of Fig. 1. The data indicate that galaxies of lower metallicities have a lower DTG and DTM than more metal-rich galaxies.

2.2 Measurements of DTG & DTM at $z>0$

Measurements of the DTG and DTM of galaxies from their emission have so far mostly been limited to the local Universe (but see Shapley et al. 2020). A new approach based on dust depletion has enabled the efficient measurement of the DTG and DTM of galaxies beyond the local Universe. This empirical method has been developed to derive the dust depletion level in the Milky Way based on gas-phase element abundances in the local part of our Galaxy (Jenkins 2009). The information from this study reveals the relative proportions of different elements to be incorporated into dust at different stages of grain growth. This method uses observed abundance patterns with assumptions about relative abundances to define depletion sequences, where the depletion effects on gas-phase abundances of all the elements is described by a single parameter. This work has been subsequently extended to both the Magellanic clouds using dedicated HST obser-

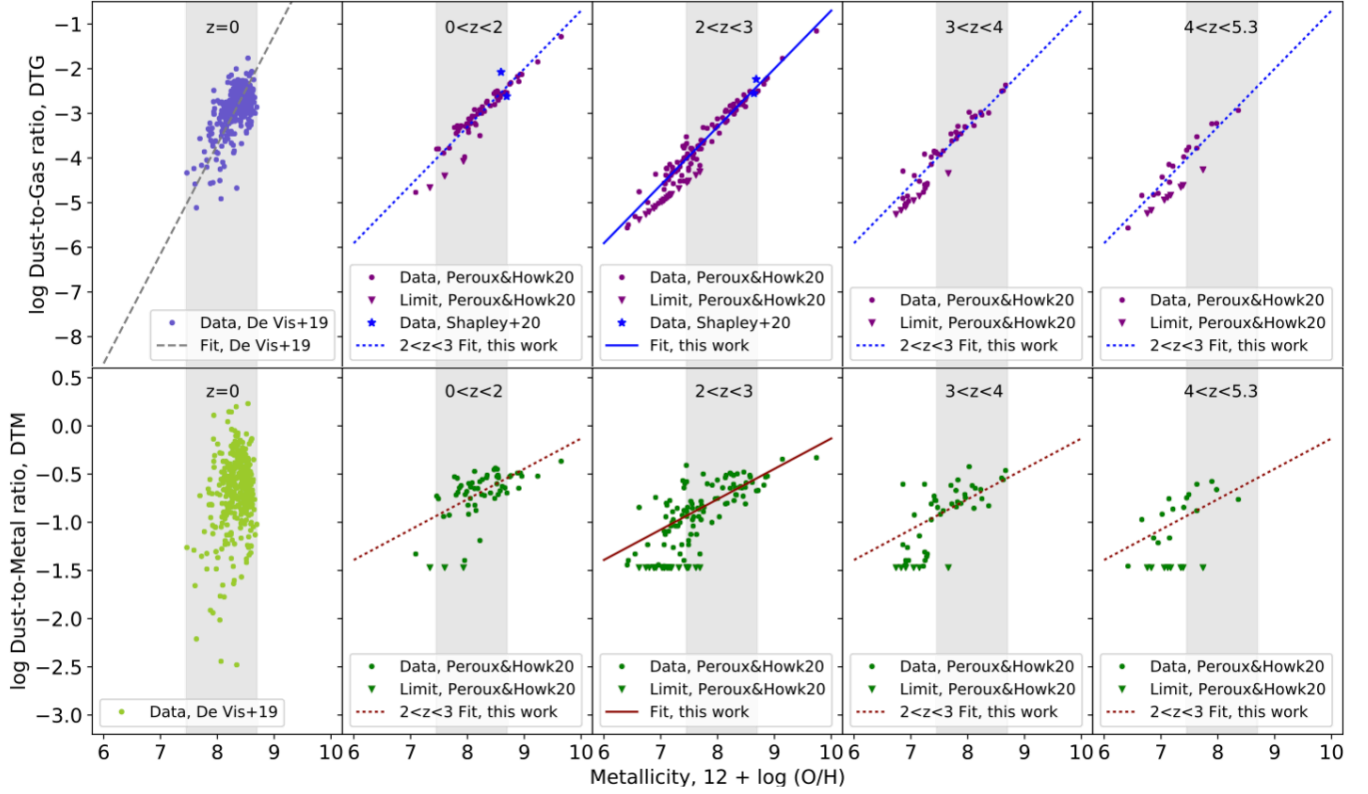


Figure 1. Observed cosmic evolution of the dust-to-gas and dust-to-metal ratios with metallicity. The grey band reproduced in all panels marks the span in metallicity of the $z=0$ data sample (detected through their emission). The $z>0$ observations (based on absorption studies) extend to both lower and higher metallicities. The DTG are tightly related to metallicity over almost 4 dex as indicated by the small scatter around the fitted linear regression. Furthermore, the fit to the observational data indicate little evolution with cosmic time of that relation at $z>0$. The scatter in the DTM measurements is larger, still providing little support for a redshift evolution of the DTM-metallicity relation.

variations of the SMC (Roman-Duval et al. 2014; Jenkins & Wallerstein 2017) and the LMC (Roman-Duval et al. 2019, 2021, 2022).

This simple scheme can be similarly implemented to derive the dust contents and metallicities of absorption-line systems that are seen in the spectra of distant quasars. Observing the gas in absorption against bright background sources provides a powerful technique to assess the gas, metal and eventually dust content of galaxies (Péroux et al. 2007; Quiret et al. 2016; Poudel et al. 2017; De Cia 2018; Berg et al. 2021). In these quasar absorbers, the minimum gas density detectable is set by the brightness of the background source. The detection efficiency is thus independent of cosmic time (Péroux et al. 2002). The high-column density gas probed in absorption is known to be strongly associated with galaxies. Multiple observational results based on Integral Field Spectroscopy have shown that the quasar absorbers are also tracing overdensities of galaxies down to low-luminosities ($L = 0.1 L_*$) (see e.g. Péroux et al. 2019; Hamañowicz et al. 2020; Dutta et al. 2021). While the physical properties of absorbing-galaxies remain to be measured statistically, early results indicate that their stellar masses range from $M_* = 10^8 - 10^{11} M_\odot$ (Augustin et al. 2018).

In large samples, the pencil-approach provides constraints on the physical properties of the average galaxy population. Absorption lines provide a measure of the surface density or column density of atoms, ions or molecules between the observer and the background source (expressed in atoms cm^{-2}). Absorption techniques directly count the number of atoms in a given phase of the gas. When

probing regions dominated by neutral atomic gas, the metallicity measurements trace only the dominant ionisation states of the metal element and hydrogen. Additionally, absorption-based gas metallicity measurements are weakly dependent on the excitation conditions making them robust estimators in comparison with emission-based measurements (Kewley et al. 2019; Maiolino & Mannucci 2019).

Jenkins (2009) provides a straightforward method to infer the level of loss of metals into dust grains, allowing one to determine the total elemental abundances to be derived from the measured gas-phase column densities. Specifically, De Cia (2018) determined corrections for the zero depletion element abundances caused by nucleosynthesis effects in such quasar absorbers, with some additional guidance from the trends seen in metal-poor stars in our Galaxy.

By using the dust sequences to assess the depletion δ for each of the elements, one can ultimately calculate their sum, the total DTG ratio for each quasar absorber (De Cia et al. 2013, 2016; Wiseman et al. 2017). These results, augmented with the latest few measurements, are available in an updated compilation in Supplementary Table 4¹ of Péroux & Howk (2020). These observations are also plotted in the four panels to the right of the first panel in the top row of Fig 1 for the following redshift ranges: $0<z<2$, $2<z<3$, $3<z<4$ and $4<z<5$. Most of the observations lie in the $2<z<3$ interval, where abundance determination in quasar absorbers can be robustly made at optical

¹ <https://www.annualreviews.org/doi/suppl/10.1146/annurev-astro-021820-120014>

wavelengths observed from the ground. Upper limits represent absorbers in which carbon is the only significant contributor to the dust content. Equally, the dust-to-metal ratio for an individual element, X , is related to its depletion: $DTM = 1 - 10^{\delta}$ (e.g., [Vladilo 2004](#); [De Cia et al. 2016](#); [Péroux & Howk 2020](#)). These observations are displayed in four panels to the right of the bottom panel of Fig 1.

2.3 Evolution of DTG & DTM extended to low-metallicity

Observations indicate that both DTG and DTM ratios are a strong function of metallicity. This result was determined based on various studies focusing on unresolved ([Issa et al. 1990](#); [Lisenfeld & Ferrara 1998](#); [Hirashita et al. 2002](#); [Draine & Li 2007](#); [Galametz et al. 2011](#); [Rémy-Ruyer et al. 2014](#); [De Vis et al. 2019](#)) and resolved ([Giannetti et al. 2017](#); [Chiang et al. 2018](#)) nearby galaxies, as well as absorption based studies focusing on high-redshift objects ([De Cia et al. 2013, 2016, 2018](#); [Zafar et al. 2013](#); [Sparre et al. 2014](#); [Wiseman et al. 2017](#)). Importantly, the quasar absorbers depletion measurements probe a new regime of low-metallicity gas which remained inaccessible in nearby galaxies (the probed metallicity range at $z = 0$ is narrower than at $z > 0$, as indicated by the grey band in Figure 1).

Our results support the conclusion that the DTM and DTG ratios are a strong function of metallicity. We find that at $z > 0$ the DTG of the absorbers increases with approximately 4 dex in the metallicity range $7 < 12 + \log(O/H) < 9$, while the DTM increases with approximately 1 dex over the same metallicity range.

Globally, a larger scatter in DTG is observed at $12 + \log(O/H) < 8$, indicating a change in the dust assembly processes at low metallicities. These findings show compelling evidence at both low and high redshifts that the DTG and DTM in galaxies are not constant, but instead are a strong function of galaxy physical property as traced for example by metallicity.

2.4 Cosmic Evolution of DTG & DTM

High-redshift measurements provide a unique opportunity to evaluate the evolution of the DTG and DTM relations with metallicity as a function of cosmic times. As detailed in Sections 2.1 and 2.2, observed quantities are derived from different techniques at $z=0$ and $z>0$. In particular, at $z = 0$ the metallicities correspond to the integrated ionised gas based on strong emission-line calibrations, whereas at $z > 0$ the metallicities are based on pencil beam absorption abundance determinations of the neutral gas. Some systematic differences between the two approaches are thus expected, although several analyses report that abundances from emission and absorption only vary by a maximum of ~ 0.6 dex ([Rahmani et al. 2016](#)).

In spite of these differences, it is noteworthy that the neutral gas measurement follows the trends seen in low-redshift galaxies at high metallicities. There is little evidence that the DTG and DTM behave differently with redshift. In the absence of a physical motivation for a specific functional form, we fit the observations with a simple power-law function as represented by the lines in Figure 1. It is remarkable to see that the DTG and DTM as measured through dust depletion from $z = 0$ and $z = 5$ are so well described by the simple power-law function (the results of the fits are tabulated in Table 1). This lack of evolution can be naturally explained as galaxies evolve along the DTG and DTM vs. metallicity relationship as a function of cosmic time.

Model	Simulation type	Condensation	Dust yields	Grain-growth model	Time scale for grain-growth depends on	Gas mass cleared of dust per SN as defined in McKee (1989)	Star formation recipe
Popping et al. (2017)	SAM	AGB, SN Type Ia and II	fixed fraction of metals: 0.15 (SN) and 0.2 (AGB)	Zhukovska (2014)	metallicity, gas surface-density	fixed mass per SN (600 (carbonaceous) and 980 (silicates)) M_{\odot}	star-formation efficiency evolves with H_2 surface density (Popping et al. 2014)
Vijayan et al. (2019)	SAM	AGB, SN Type II	fixed fraction for SN (0.15) and AGB yields from Ferrarotti & Gail (2006)	Zhukovska (2014)	dust abundance	fixed mass per SN (1200 M_{\odot})	star-formation efficiency evolves with gas mass and galaxy disc dynamical time (Henriques et al. 2015)
Triani et al. (2020)	SAM	AGB, SN Type II	fixed fraction of metals: 0.15 (SN) and 0.2 (AGB)	Dwek (1998)	metallicity	scales negatively with metallicity (Yamasawa et al. 2011)	scales linearly as a function of H_2 surface density (Triani et al. 2020)
Hou et al. (2019)	hydrodynamical	SN Type II	yield tables from Nozawa et al. (2006)	Hirashita & Kuo (2011)	metallicity and DTG (with fixed dense gas fraction)	ISM density (see Aoyama et al. 2017)	scales linearly with local gas density (Aoyama et al. 2017)
Li et al. (2019)	hydrodynamical	AGB, SN Type II	fixed fraction of metals: 0.15 (SN) and 0.2 (AGB)	Dwek (1998)	temperature, density, metallicity	fixed mass per SN ($\sim 2040 M_{\odot}$)	scales with H_2 density and disc dynamical time (Davé et al. 2019)
Graziani et al. (2020)	hydrodynamical	AGB, SN Type II	yield tables from Schneider et al. (2004) and Bianchi & Schneider (2007) (SN) and Ferrarotti & Gail (2006) and Zhukovska et al. (2008) (AGB)	de Bennassuti et al. (2014)	temperature, density, metallicity	fixed mass per SN ($\sim 2040 M_{\odot}$)	scales with local gas density (Springel et al. 2005a)

Table 2. Overview of the implementation of dust-chemistry of the various models discussed in this work. All these properties contribute to the physics encoded in the relation between DTG or DTM and gas-phase metallicity takes.

3 MODEL DESCRIPTIONS

We now compare the DTG and DTM derived from observations to a number of cosmological semi-analytic and hydrodynamical simulations of galaxy formation and evolution. These simulations were selected to include the tracking of dust production and destruction for a full cosmological volume over a large redshift range (partially) overlapping with the observational sample. The predictions by the simulations by [McKinnon et al. \(2018\)](#) were unfortunately not available to us. Predictions by the [Kannan et al. \(2021\)](#) model focus on redshift $z > 5.5$, for which there are no observations to compare to yet.

All discussed models include typical processes that control the dust enrichment of the ISM, such as the condensation of metals in the stellar ejecta of SNe and AGB stars, dust mass growth through the accretion of metals onto dust grains, the destruction of dust in the vicinity of SNe due to shocks (accounting for the effects of correlated SNe: SNe exploding in existing super-bubbles created by previous SNe in the association) and the destruction of dust in hot gas due to thermal sputtering. Since the reversed shock in supernova acts on scales smaller than resolved in these simulations, the impact of the reversed shock on dust yields is taken into account by an effective yield for SNe (rather than the yield before dust is destroyed by a reversed shock). Furthermore they all include astration (dust that is destroyed while it is participating in the formation of new stars) and the flows of dust into and out of galaxies due to stellar and AGN winds and cold gas accretion. None of these models explicitly model the surviving rate of dust in stellar and AGN winds.

Below we provide a brief overview of the details of dust modelling in the various models considered in this work and we provide a summary of the relevant parameters in Table 2. We refer the reader to the original papers for a detailed description.

3.1 Semi-analytic models

3.1.1 *Popping et al. (2017)*

The dust-evolution model of [Popping et al. \(2017\)](#) builds upon the SANTA CRUZ semi-analytical model ([Somerville & Primack 1999](#); [Somerville et al. 2008, 2015](#); [Popping et al. 2014](#)). The model includes the condensation of dust in the ejecta of Type Ia and II supernovae and asymptotic giant branch (AGB) stars. The model adopts the prescription from [Zhukovska \(2014\)](#) to model grain growth in the molecular ISM with a timescale that depends on the gas phase metallicity and surface density of the dense ISM. Grain-growth only takes place in the molecular phase of the ISM, calculated using the [Gnedin \(2010\)](#) partitioning recipe. The destruction of dust is modelled following [Dwek & Scalo \(1980\)](#) and [McKee \(1989\)](#) assuming a fixed mass of gas cleared of dust per SN event. The model furthermore includes astration, thermal sputtering of dust and the in- and outflow of dust into the ISM.

3.1.2 *Vijayan et al. (2019)*

The dust chemistry model presented in [Vijayan et al. \(2019\)](#) is implemented within the L-GALAXIES semi-analytic model ([Henriques et al. 2015](#)). The model includes the condensation of dust in SN II and AGB stars, grain-growth in the ISM, destruction of dust by SNe, astration and the in- and outflow of dust into the ISM. [Vijayan et al. \(2019\)](#) assume a timescale for the accretion of metals onto dust-grains in the molecular ISM that scales with the dust-abundance of

the cold gas, calibrated to match observed dust masses at high redshifts. The molecular phase of the ISM is calculated using the [McKee & Krumholz \(2010\)](#) partitioning recipe for atomic and molecular gas. The destruction of dust follows the work of [Dwek & Scalo \(1980\)](#) and [McKee \(1989\)](#), assuming a fixed mass of gas cleared of dust per SN event. In the [Vijayan et al. \(2019\)](#) model all dust that is transferred to the hot halo is destroyed directly.

3.1.3 *Triani et al. (2020)*

[Triani et al. \(2020\)](#) implemented a detailed dust prescription in the Semi-Analytic Galaxy Evolution (SAGE, [Croton et al. 2016](#)) model. This version of the model, called DUSTY SAGE, includes condensation of dust in the ejecta of Type II supernovae and AGB stars, grain growth in molecular clouds, destruction by supernovae shocks, and the removal of dust from the ISM through astration, reheating, inflows, and outflows ([Triani et al. 2020](#)). The authors adopt the procedure presented in [Dwek \(1998\)](#) to model grain growth in the molecular ISM. The molecular fraction of the ISM is calculated using the [Blitz & Rosolowsky \(2006\)](#) partitioning recipe for atomic and molecular gas. The destruction of dust by SNe is modeled following [Dwek & Scalo \(1980\)](#) and [McKee \(1989\)](#), assuming that the mass of dust swept up per SN event depends on the gas-phase metallicity (following [Yamasawa et al. 2011](#)), such that more dust is swept up in metal-rich environments.

3.2 Hydrodynamical models

3.2.1 *Hou et al. (2019)*

[Hou et al. \(2019\)](#) presents predictions for the evolution of DTG and DTM by making use of the cosmological simulation presented in [Aoyama et al. \(2017\)](#) and [Hou et al. \(2017\)](#), a modified version of the GADGET-3 *N*-body/smoothed particle hydrodynamic code presented in [Springel et al. \(2005b\)](#). The model considers dust production in Type-II SNe and the accretion of metals onto dust gains in the dense ISM following [Hirashita & Kuo \(2011\)](#), similar to [Dwek 1998](#)). The timescale for dust accretion depends on the metallicity and DTM of the gas. Dust accretion only occurs in the dense ISM and it is assumed that the ISM has a fixed fraction of dense gas of 0.1. The destruction of dust by SN shocks is modeled following [McKee \(1989\)](#), where the gas mass swept up per SN event depends on the gas density of the particle. Additionally, dust is destroyed by thermal sputtering.

The [Hou et al. \(2019\)](#) model is the only one presented in this work that includes a dust size distribution and divides dust in two type of grains, large and small. Small and large grains have different efficiencies for the accretion of metals onto dust grains and the destruction of dust by SN shocks. Furthermore, the model includes the coagulation of small grains and the shattering of large grains (see also [Li et al. 2020](#)).

3.2.2 *Li et al. (2019)*

[Davé et al. \(2019\)](#) includes the tracking of dust production and destruction as a part of the SIMBA cosmological simulation, built upon the GIZMO cosmological gravity plus hydrodynamic solver ([Hopkins 2015](#)). [Li et al. \(2019\)](#) presents the evolution of the DTG and DTM predicted by the SIMBA simulation. The model for dust production and destruction includes the condensation of dust in the ejecta of AGB stars and Type-II SNe and the accretion of metals onto dust grains (following [Dwek 1998](#)) assuming a accretion timescale that

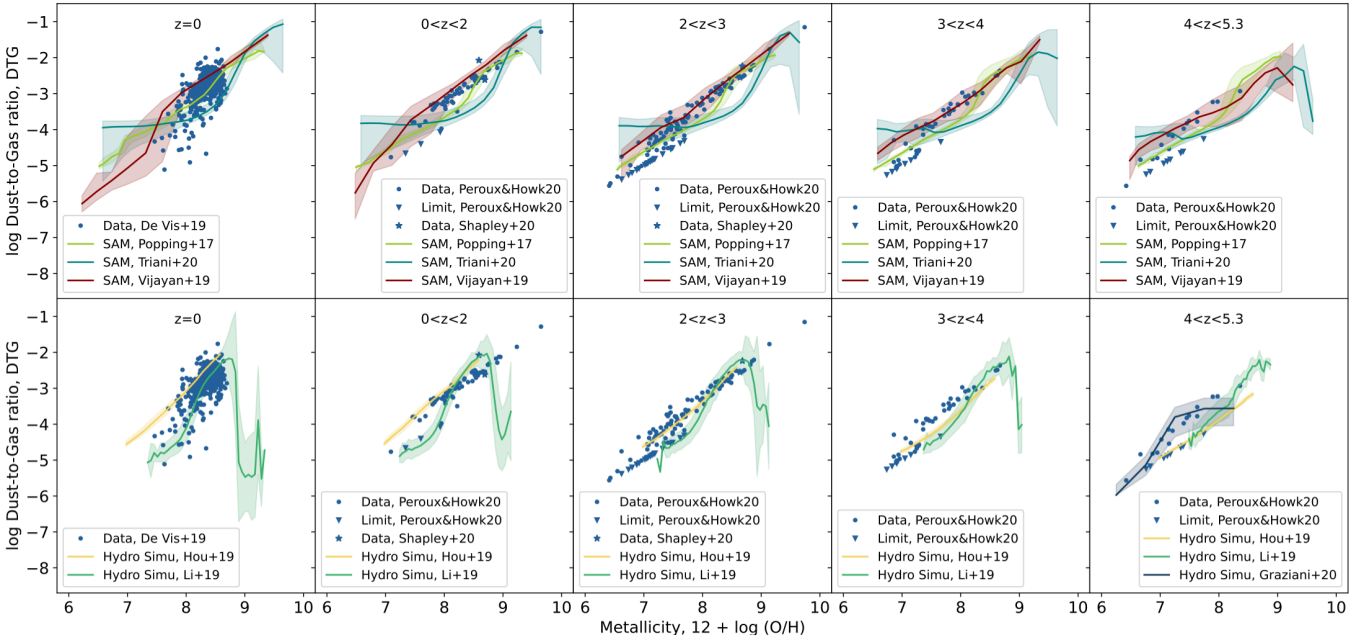


Figure 2. Observed and modeled evolution of dust-to-gas ratios with metallicity. The data points are identical to the top row of Figure 1. The lines in the top row of this figure depict three different semi-analytical models with associated $1-\sigma$ error estimates, while the lines in the bottom row depict three different hydro-dynamical models. The models reproduce the observed DTGs with varying degree of success.

depends on the temperature, metallicity and density of the ISM. Metal accretion can in theory take place in every particle in the simulation, although it will be less efficient in the diffuse ISM due to the density dependence. The model furthermore includes thermal sputtering of dust and the destruction of dust in SN blast waves (Dwek & Scalo 1980; McKee 1989), assuming a fixed mass of gas swept up per SN event. Dust is additionally destroyed in hot winds, due to X-ray heating and through astration.

3.2.3 *Graziani et al. (2020)*

Graziani et al. (2020) presents *DUSTYGADGET*, a code following the evolution of dust grains in different phases of the ISM and the spreading of dust and atomic metals by galactic winds throughout the circum- and intergalactic medium. This code is built upon the *GADGET* (Springel et al. 2005b) model and extensions presented in Tornatore et al. (2007b,a) and Maio et al. (2009). The model follows the condensation of dust in population III SN, population II/I core-collapse SNe and AGB stars using yield tables from Schneider et al. (2004), Bianchi & Schneider (2007) and Ferrarotti & Gail (2006) and Zhukovska et al. (2008), respectively. This is the only of the discussed models that adopts dust-yield tables for both SNe and AGB stars, describing the condensation of dust as a function of the stellar mass and metallicity, rather than a fixed condensation efficiency independent of stellar properties. The *Graziani et al. (2020)* model describes the accretion of metals onto dust grains assuming a timescale that depends on the density, metallicity and temperature of a star-forming SPH particle and the destruction of dust by supernova shocks following McKee (1989) with a fixed mass of dust cleared from the ISM per SN (with varying efficiencies for core-collapse and pair-instability SNe). Metal accretion can only take place in cold and star-forming particles, which is different from the implementation of Li et al. (2019). Lastly, the model includes grain sputtering in the

hot plasma and astration. The *Graziani et al. (2020)* model is evolved only down to $z = 4$ due to computational limitations.

4 CONFRONTING DATA TO MODELS

4.1 Dust-to-gas ratio

Figure 2 shows the observed DTG of galaxies as a function of their gas-phase metallicity (as presented in the top row of Figure 1). The different columns represent different redshift bins, whereas the various lines mark the predictions by the respective models discussed in Section 3. The top row of Figure 2 shows a comparison between observations and model predictions by semi-analytical models, whereas the bottom row shows the comparison with hydrodynamic models.

It is remarkable that despite the different implementations between the various models for baryonic physics (e.g., the formation of stars, the accretion of gas onto galaxies, the growth of black holes and stellar and AGN feedback), the predicted relation between DTG and gas-phase metallicity is roughly consistent between many of the models. The Popping et al. (2017), Triani et al. (2020), Li et al. (2019) and Graziani et al. (2020) models predict a relation between DTG and gas-phase metallicity that takes an ‘s-shape’. The Hou et al. (2019) and Vijayan et al. (2019) models on the other hand predict a roughly linear relation. The quick rise in DTG around $12 + \log(O/H) \sim 8$ (8.5 for Triani et al. 2020) is driven by the onset of accretion of metals onto dust grains as an important channel for the growth of dust mass (see for example Popping et al. 2017 and Triani et al. 2020). Furthermore, except for Hou et al. (2019), all other models discussed in this work predict that the relation between DTG and metallicity is roughly constant with time. A constant relation between gas-phase metallicity and DTG is in apparent agreement with observations (Figure 1, De Cia et al. 2016; Péroux & Howk 2020; Shapley et al.

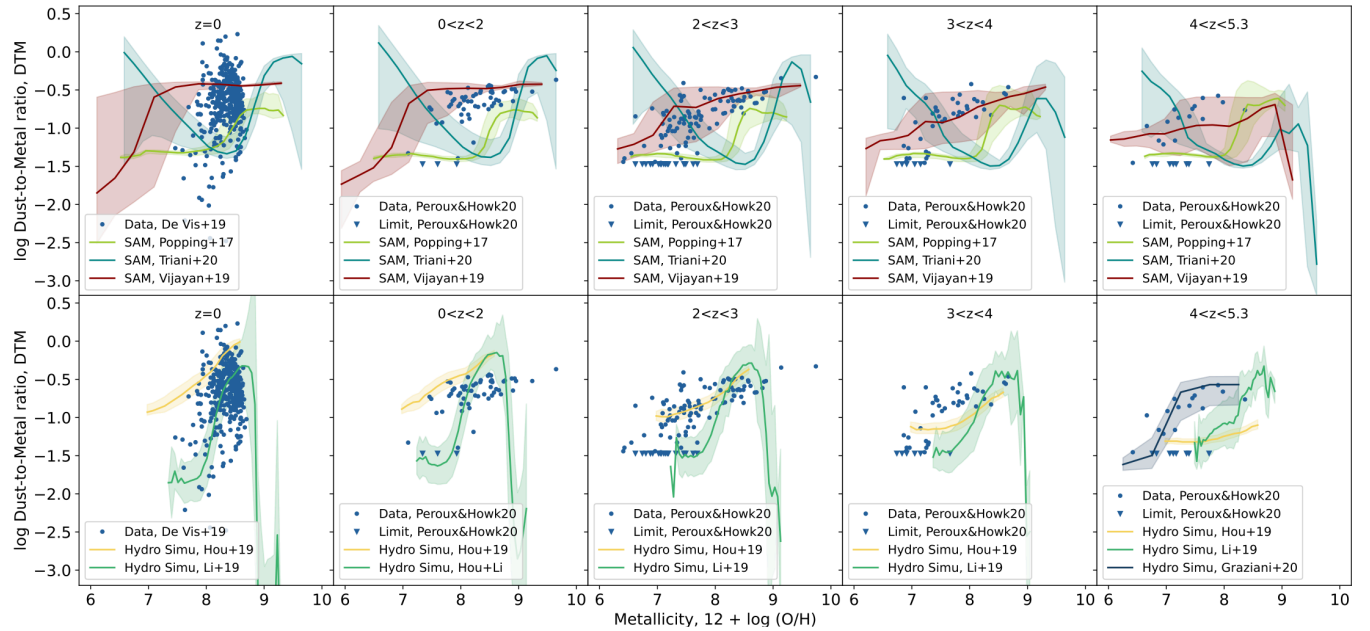


Figure 3. Observed and modeled evolution of dust-to-metal ratios with metallicity. The data points are identical to the bottom row of Figure 1. Similar to Figure 2, the lines in the top row depict three different semi-analytical models with associated $1-\sigma$ error estimates, while the lines in the bottom row depict three different hydro-dynamical models. The DTMs are reproduced by the models with a varying degree of success with vastly different predictions at fixed redshifts and for the cosmic evolution of the relation between DTM and metallicity.

2020). The Hou et al. (2019) model predicts that the normalization of this relation increases with cosmic time.

The models discussed in this work reproduce the observed relation between DTG and gas-phase metallicity with a varying degree of success. Although all models reproduce part of the probed dynamic range in metallicity, a close look at the individual models does show differences. The Triani et al. (2020) model predicts a DTG at metallicities around $12 + \log(O/H) \sim 8 - 9$ that is about half a dex lower than the observations, independent of redshift. At lower metallicities the Triani et al. (2020) model predicts a DTG that is up to a dex too high. The Popping et al. (2017) and Li et al. (2019) models predict a DTG at $12 + \log(O/H) \sim 8$ that is ~ 0.25 dex lower than the observations. The Vijayan et al. (2019) model reproduces the DTG of galaxies with a gas-phase metallicity larger than $12 + \log(O/H) = 8$ well, but predicts a DTG that is about half a dex too large at lower metallicities. The predictions by the Hou et al. (2019) model for the relation between DTG and gas-phase metallicity agree well with the observations for galaxies at $z < 3$, but the predicted DTG is up to a 0.5 - 1 dex too large at higher redshifts. The predictions by Graziani et al. (2020) model at $z > 4$ are in excellent agreement with the observed DTG, but the non-detections fall outside of the typical one-sigma scatter predicted by this model. The Li et al. (2019) and Triani et al. (2020) models both show a steep drop in the DTG for galaxies at the highest metallicities, corresponding to quenched galaxies not included in the observational sample.

4.2 Dust-to-metal ratio

In Figure 3 we present the relation between the DTM and metallicity of galaxies at various redshifts. We find significant differences in the predictions by the various models for the relation between DTM and gas-phase metallicity. The Popping et al. (2017), Vijayan et al. (2019) and Li et al. (2019) models all predict a clear 's-shape'. Similar to the

DTG the quick rise in DTM at a metallicity of $12 + \log(O/H) \sim 8$ is driven by the onset of accretion of metals onto dust grains as a channel for dust formation. The Graziani et al. (2020) model also predicts an 's-shape' at $z > 4$, but the quick rise in DTM already occurs at a metallicity of $12 + \log(O/H) \sim 7$. The Hou et al. (2019) model predicts a roughly linear relation between DTM and gas-phase metallicity at $z < 2$ and an exponential relation at higher redshifts. The Triani et al. (2020) model on the other hand predicts that the DTM of galaxies decreases with increasing gas-phase metallicity up to $12 + \log(O/H) = 8$ and increases again at higher metallicities.

Besides differences in the shape of the relation between gas-phase metallicity and DTM the various models also predict a different redshift evolution. The relation predicted by Popping et al. (2017), Triani et al. (2020) and Li et al. (2019) is fairly constant with time, whereas the Vijayan et al. (2019) and Hou et al. (2019) models predict that the relation between gas-phase metallicity and DTM becomes steeper as a function of cosmic time.

We now continue to review the successes and shortcomings of the various models when comparing their predictions to the observations. The Popping et al. (2017) model predicts a DTM that is up to ~ 0.75 dex too low, independent of gas-phase metallicity. Similar to the observations, the Popping et al. (2017) predicts a quick rise in DTM but at a metallicity of $12 + \log(O/H) \sim 8$, rather than a metallicity of $12 + \log(O/H) \sim 7$ as suggested by the observations. The Triani et al. (2020) model predicts a decrease in DTM as a function of gas-phase metallicity at $12 + \log(O/H) < 8$, whereas the data suggests an increase in DTM. At higher metallicities the Triani et al. (2020) model predicts a DTM that is between one and 0.2 dex lower than the observed DTM. The predictions by the Vijayan et al. (2019) model are in good agreement with the observations at $z > 2$. At redshifts $z < 2$ this model predicts a DTM that is about 0.25 dex too high for galaxies with $12 + \log(O/H) > 8$, suggesting the quick rise in DTM occurs at too low metallicities. The Li et al. (2019) model

reproduces the observations fairly well at $z < 2$, but predicts a DTM that is typically too low at higher redshifts (by 0.5-0.75 dex). The predictions by [Hou et al. \(2019\)](#) model are in decent agreement with the observations at $2 < z < 3$. At redshifts $3 < z < 5$ the predicted DTM is up to 0.5 dex too low, whereas at $z < 2$ the predicted DTM is up to 0.5 dex too large. The predictions by the [Graziani et al. \(2020\)](#) model at $z > 4$ are in good agreement with the observed DTM.

4.3 Differences between models explained

There are clear differences between the various model predictions and large discrepancies between the model predictions and observations. None of the presented models succeeds in simultaneously reproducing the relation between DTG or DTM and gas-phase metallicity over the full redshift and metallicity range covered by the observations. Overall, this suggests that the DTG and DTM of galaxies are an excellent test for the success of a model that follows the formation and destruction of dust. The differences between models also provide relevant clues to how various implementations of dust physics control the buildup of dust in galaxies.

The various models discussed in this work all predict a different critical metallicity at which the DTG and DTM rapidly increase. For some models, this critical metallicity evolves with redshift. The critical metallicity is set by the efficiency of dust growth *and* inversely by the star-formation timescale of galaxies ([Asano et al. 2013](#), [Zhukovska 2014](#), see also [Feldmann 2015](#)). When the timescale for star formation is longer, metals have more time to accrete onto dust grains until the metallicity increases to a higher value due to star-formation driven metal enrichment. The recipes employed for dust growth in the ISM between the different models discussed in this work are all similar, which suggests that the change in critical metallicity between models (and even with redshift for the individual models) are driven by changes in the timescale of star-formation. It is beyond the scope of this work to reconstruct the timescale for star-formation in every model as a function of galaxy properties and time, however, we do note that the various models all adopt different recipes for star-formation that result into different timescales (up to an order of magnitude, see the last column of Table 2). Interestingly, the [Popping et al. \(2017\)](#), [Triani et al. \(2020\)](#) and [Li et al. \(2019\)](#) models all predict a critical metallicity at which the DTG and DTM rapidly increases that is higher than suggested by the observations (indicative of a star-formation time scale that is too short) and these are the only three models discussed in this work that adopt a star-formation recipe directly tied to the molecular gas budget in galaxies.

Besides the timescale of star-formation, there are a number of additional physical drivers for the differences in the predicted DTM and DTG. [Hou et al. \(2019\)](#) predict a redshift evolution in the relation between gas-phase metallicity and DTG and DTM. This evolution is likely driven by their assumption of a dense gas fraction of 10%, whereas the other models take the molecular hydrogen fraction of the cold gas as the dense fraction (which is thought to be of the order 50% and higher for massive galaxies at early times, e.g., [Lagos et al. 2011](#); [Fu et al. 2012](#); [Popping et al. 2014, 2015](#)). By adopting a dense gas fraction of 0.1, only small amounts of dust can be formed through the accretion of metals onto dust grains. This naturally slows down the buildup of dust in the ISM at early times, resulting in a strong evolution in the DTG at lower redshifts, rather than reaching an equilibrium between grain-growth and destruction early on (as in for example [Popping et al. 2017](#)).

The [Vijayan et al. \(2019\)](#) model also predicts a strong redshift evolution in the relation between DTM and gas-phase metallicity (this evolution is not so obvious in the relation with DTG). [Vijayan et al.](#)

(2019) adopted a model for the accretion of metals onto dust-grains similar to [Popping et al. \(2017\)](#), based on the work by [Zhukovska \(2014\)](#). One of the fundamental differences between the two models is that [Popping et al. \(2017\)](#) calculate the timescale for metal accretion (among others) as a function of gas-phase metallicity (see also [Li et al. 2019](#)), whereas [Vijayan et al. \(2019\)](#) calculate this as a function of the dust-abundance of the dense ISM. This can make a significant difference to the dust growth rate at early times. As a consequence, it takes longer for galaxies to reach the saturation limit in the DTM, explaining the observed redshift evolution compared to for instance [Popping et al. \(2017\)](#) and [Li et al. \(2019\)](#).

A clear difference in the implementation of dust physics in the various models is the use of yield tables to describe the dust enrichment of the ISM by AGB stars and supernovae. The [Popping et al. \(2017\)](#), [Li et al. \(2019\)](#) and [Triani et al. \(2020\)](#) models assume a fixed dust yield for all AGB stars and SNe, motivated by either observations or theoretical models. The [Vijayan et al. \(2019\)](#) model assumes a fixed condensation fraction of metals into dust for SNe and uses yield tables for AGB stars. The [Hou et al. \(2019\)](#) model adopts yield tables for dust enrichment by SNe, but ignores the effect of AGB stars. The [Graziani et al. \(2020\)](#) model is the only model discussed in this work that adopts yield tables for dust enrichment by AGB stars and SNe. The [Graziani et al. \(2020\)](#) model best reproduces the $z > 4$ observational constraints between DTG and DTM and metallicity, although this can not be fully ascribed to the use of yield tables as other processes such as the destruction of dust and the accretion of metals onto dust grains also play a relevant role. Nevertheless, including yield tables will be a relevant improvement for models that track the buildup of dust in galaxies, especially in the regimes where dust growth in the ISM is not yet a dominant contributor to the dust budget of galaxies such as low-metallicity environments and the early Universe.

5 DISCUSSION

5.1 No cosmic evolution in galaxy dust properties with metallicity

We found that the DTG and DTM are a strong function of galaxy properties as traced for instance by metallicity and that there is little evolution (at $z < 5.3$) in this function, i.e., galaxies evolve along the relation between DTG or DTM and metallicity (Section 2 and Figure 1). The latter implies that the dust-chemistry time-scales at play must be short enough for said relations to be in place within galaxies already at $z \sim 5$, when the Universe was only ~ 1.1 Gyr old. If grain growth through the accretion of metals onto dust grains is to play an important role in the early Universe for metal-enriched galaxies (e.g., [Mancini et al. \(2015\)](#), [Popping et al. \(2017\)](#), c.f., [Ferrara et al. 2016](#)) the grain-growth timescale must be significantly shorter than 1.1 Gyr. Furthermore, the lack of evolution also suggests that the balance between dust formation and destruction (as well as dust-poor inflows and dust-enriched outflows) is constant as a function of metallicity and therefore closely coupled to metal enrichment, i.e., the star-formation history rather than other external parameters ([Wendt et al. 2021](#)).

Importantly, the relation between DTG and metallicity has implications for studies of the cosmic evolution of cold gas based on dust mass measurements. These works infer the gas-mass of galaxies from their estimated dust mass observed in the far-infrared and mm domains. In recent years, single millimeter dust-continuum measurements in particular have been used as estimators of galaxy cold gas masses (see for example [Scoville et al. 2017](#), [Kaasinen et al. 2019](#)). In

some cases these recipes account for changes in the DTG as a function of metallicity (Bertermes et al. 2018; Wang et al. 2022), but not always. The robustness of such dust-based gas mass estimates will be improved by using the DTG-metallicity relation tabulated in Table 1. These refined results will affect in particular the studies focusing on low-mass galaxies and galaxies during the epoch of reionisation.

5.2 DTG and DTM as a constraint for models

The tension between the predictions by the various models and the observational constraints from absorption studies demonstrate that the DTG and DTM of galaxies should be used as a stringent constraint for models that include dust chemistry. Indeed, none of the models succeeds in reproducing the derived values over the entire range in redshift and gas-phase metallicity now probed by the observations. Besides reproducing the exact shape of the various relations, some of the models also fail to reproduce the wide scatter observed.

Galaxy formation models are complex indeed, including different recipes for all the baryonic physics that is relevant to describe the evolution of galaxies within their cosmological environments (e.g., the accretion and cooling of matter onto galaxies, the formation of stars, black hole growth, stellar and black hole feedback, metal enrichment, see the reviews by Somerville et al. 2015 and Naab & Ostriker 2017). As a consequence, it is sometimes complicated to understand why one model reproduces a certain observation better than another. Due to the close link between dust and gas metals in galaxies (dust originates from metals) the situation is more informative for the dust budget in galaxies compared to their metal content. This assumes that dust and metals follow each other closely in flows of gas, for example in galactic outflows. We found that differences in the relation between DTG or DTM and gas-phase metallicity can be well explained by the different implementations of the dust-chemistry model in combination with the timescale for star formation (see Section 4.3).

We find that the critical metallicity at which the DTG and DTM of galaxies rapidly increases predicted by the Popping et al. (2017), Triani et al. (2020) and Li et al. (2019) is too large at $z > 2$. This is suggestive of a star-formation timescale in these simulations that is too short. Alternative approaches to contribute to bringing the models in better agreement with the data include unphysically high condensation efficiencies in stellar ejecta of 100 per cent (as explored in Popping et al. 2017) or timescales for the accretion of metals onto dust grains that are unrealistically short. A heavily reduced efficiency of dust destruction by SN blast waves at lower metallicities could also contribute, but is in strong disagreement with models (Hu et al. 2019, Martínez-González et al. 2019, see also the discussion in Ferrara & Peroux 2021), this may not contribute enough to resolve the tension (e.g., when turning dust-destruction off in the Popping et al. 2017 models the upturn in the DTM occurs at metallicities only ~ 0.2 dex lower than for the fiducial model with dust destruction, indicating that not enough dust is produced to begin with in low-metallicity galaxies or that the galaxies are enriched too quickly). What this ultimately demonstrates, is that the relations of galaxies' DTG and DTM with gas-phase metallicity provide a new and unique approach to not only constrain the dust-physics in galaxies, but also the timescale of star-formation at different cosmic epochs.

5.2.1 Caveats on the implementation of dust physics

The physics of dust formation and destruction is in reality significantly more complex than can be captured in the various sub-grid

recipes adopted in models and is also affected by various physical phenomena not included in the discussed cosmological simulations at all. In Section 4.3 we attempted to highlight how the differences between model predictions can be explained by their implementations for the formation and destruction of dust. It is nevertheless relevant to take into account some of the current caveats or shortcomings in the implementations of dust-physics as these may also play a relevant role in shaping the evolution of dust in galaxies and the agreement with observations. Below we discuss a number of examples relevant for the presented works.

As a first example we can take the accretion of metals onto dust grains which is thought to take place in the cold ISM of galaxies. The models discussed in this work do not include the chemical networks to cool down the gas to typical temperatures and densities of the molecular ISM (well below the temperatures reached in cosmological simulations of 10000 K). Instead the models rely on sub-grid approaches to calculate the efficiency of metal accretion on dust grains and make sub-grid choices to decide in which fraction of the ISM of galaxies grain growth may take place (e.g., in a fixed dense gas fraction of 0.1 as implemented in Hou et al. 2019 or in star-forming SPH particles as implemented in Graziani et al. (2020)). It is not yet clear if these choices are close to reality and the success of one over the other may therefore not necessarily imply a better physical description of the dust physics at play. A coarse description of the cooling of the ISM not only affects the efficiency of grain-growth but also the timescales for the formation of stars. The inclusion of chemical networks to better describe the temperature and density conditions of the ISM in simulations (e.g., Kannan et al. 2021) may therefore have a non-negligible impact on the formation of dust and the DTG and DTM of galaxies.

As a second example we can take the destruction of dust by supernovae. Dust destruction occurs close around supernovae when the reversed shock passes (e.g., Bocchio et al. 2016) and at the scale of the ISM when the supernova shock wave passes through the ISM. The latter is implemented in the simulations (roughly following the approach from McKee 1989, but the gas mass cleared of dust has a dependence on the density of the ISM (Temim et al. 2015) which is not included in the models. The former process is accounted for in the simulations by adopting effective yields for supernovae (corresponding to the dust condensation efficiency after the reversed shock passed). The true effective yield can in reality not be captured by a single number and will depend on a number of parameters not resolved in cosmological simulations. The systematic uncertainties associated to both destruction processes are likely also affecting the buildup of dust in galaxies.

As a last example, somewhat related to the first example, we can take the close coupling between radiation and dust. The exposure of grains to different types of radiation fields from different stars and at different wavelengths has a strong impact on grain surface chemistry (e.g., Ivlev et al. 2015). The presence of charged dust-grains has an impact on the evolution of the multiphase ISM and affects the grain sizes (Glatzle et al. 2022). These effects ultimately play a role in for example the efficiency of dust formation through the accretion of metals. More specifically, some works have discussed that metals accreted on the surface of dust grains in the coldest ISM (10-20 K) are captured in icy mantles. These mantles are thought to be photo-desorbed once they return to the diffuse ISM making grain-growth in the coldest ISM an inefficient channel for the formation of dust (Ferrara et al. 2016; Ceccarelli et al. 2018).

5.3 The next steps

This work includes the determination of the DTG and DTM of galaxies as obtained through absorption studies. By nature, these studies probe the DTG and DTM of a galaxy along an individual sightline in the neutral ISM, rather than measuring the integrated quantities. A complementary approach to study the DTG and DTM of galaxies would be to measure their dust and gas content and metallicity through emission studies. [Shapley et al. \(2020\)](#) utilised ALMA dust continuum and CO observations to measure the dust content and gas content of 4 galaxies with metallicity measurements based on rest-optical emission lines, and found that the DTG of galaxies at $z \sim 2$ with solar metallicity is similar to the DTG found in local galaxies with solar metallicity. Extending such observations to probe a broader dynamic range in gas-phase metallicity would be important to obtain an alternative measurement of the relation between metallicity and DTG and probe the importance of systematics between various methodologies to measure the DTG and DTM of galaxies. Additionally, future modeling work could focus on mocking the absorption studies, drawing the metallicity, DTG and DTM of galaxies from individual sightlines in the modeled volume.

We have shown that measurements of the dust properties of galaxies through absorption studies provide important constraints for galaxy evolution models. Most models discussed in this work predict a change in slope in the relation between DTG or DTM with gas-phase metallicity which is not evident in the absorber data. A larger sample of observational constraints at $12 + \log(O/H) < 8$ is required to shed further light on this. Furthermore, a statistically more robust sample of absorbers at $z > 4$ will provide key information about the redshift evolution of the discussed relations and prove to be essential to estimate the dust timescales necessary for galaxies to reach a balance in the dust-chemistry which leads to the non-evolution of those relations.

We also note that further studies looking at the global dust properties as a function of other galaxy physical properties would also be welcome. In particular, a detailed knowledge of the star formation rate and stellar mass associated with the quasar absorbers will enable a fairer comparison with some of the models presented here. Specifically, some of the model s-shape relations occur because the nature of the ISM of large main-sequence galaxies significantly differs from dwarf galaxies. Indeed, these galaxy types show varying structure of ISM environments and are affected differently by chemical, radiative and mechanical feedback effects. In the future, a more detailed comparison will come from drawing galaxies through sightlines and even mocking their emission using radiative transfer codes (although the various assumptions that need to be made when applying radiative transfer codes do introduce additional systematic uncertainties).

In this work we focused on the dust-abundance of galaxies. Nevertheless, the depletion pattern of individual elements can be obtained through absorption studies ([Mattsson et al. 2019](#)) and captures key information on the type of dust present and their formation channels. For example, [Dwek \(2016\)](#) argues that iron in galaxies is more depleted than can be explained by dust condensation in the ejecta of AGB stars and core-collapse supernova alone, suggesting that iron in the ISM depletes onto dust grains. A careful accounting of metal depletion in simulations compared to observations has the potential to test the composition of dust predicted by models and the contribution to the total dust budget by the various formation channels. This will push galaxy formation models to improve their dust chemistry recipes for individual elements, for instance by including dust yield tables for AGB stars and supernovae (e.g., [Ferrarotti & Gail 2006](#), [Bianchi & Schneider 2007](#) and [Mattsson et al. 2010](#), see for in-

stance [Graziani et al. 2020](#)) rather than assuming fixed condensation efficiencies.

Lastly, the disagreement between models and observations concerning the DTG and DTM of galaxies as a function of their metallicity (see Figures 2 and 3) asks for a careful re-evaluation of the implementation in the discussed models of the production and destruction of dust in concert with the timescale for star-formation. This is especially relevant if similar type of comparisons based on drawing sightlines in the simulated volumes will result in a similar disagreement. The data and comparisons presented in this work provide a unique approach to breaking the degeneracy between dust-chemistry implementation and the timescale for star-formation, with significant consequences for the modeling of the buildup of stellar mass over cosmic time.

6 SUMMARY AND CONCLUSION

In this work we presented a comprehensive overview of the relation between the metallicity and the dust-to-gas (DTG) and dust-to-metal (DTM) ratio of galaxies from $z = 0$ to $z = 5$. In particular, we gathered the latest observational measurements from studies of luminous galaxies at $z = 0$ ([De Vis et al. 2019](#)), from absorption studies covering a redshift range $0 < z < 5$ ([De Cia et al. 2016](#); [Wiseman et al. 2017](#); [Péroux & Howk 2020](#)), and from a study probing the DTG of luminous galaxies at $z \sim 2$ ([Shapley et al. 2020](#)). The observations are compared to predictions by a number of semi-analytic ([Popping et al. 2017](#); [Vijayan et al. 2019](#); [Triani et al. 2020](#)) and hydrodynamical ([Li et al. 2019](#); [Hou et al. 2019](#); [Graziani et al. 2020](#)) models. Our main results include:

- A linear relation exists between the DTG and metallicity of the observed galaxies across cosmic time. Only at metallicities less than $12 + \log O/H < 8$ are there hints of an increased scatter. There is little to no evolution in the observed relation from $0 < z < 5$. Similarly, the relation between DTM and gas-phase metallicity is also fairly constant with time. The lack of evolution in the relations between DTG and DTM and metallicity are indicative of a balance between the formation and destruction of dust, already at $z = 5$ when the Universe was 1.2 Gyr old. The $z = 0$ data shows a different slope, but we note that the dynamic range in metallicity covered at $z = 0$ is narrower than at higher redshifts.

- None of the presented theoretical models is able to successfully reproduce the DTG and DTM of galaxies as a function of their metallicity over the entire redshift range considered in this work.

- The observations suggest that the timescale for star-formation in the [Popping et al. \(2017\)](#) and [Li et al. \(2019\)](#) is too short, whereas the timescale for star-formation in [Vijayan et al. \(2019\)](#) at $z < 2$ is too long. The observations furthermore suggest that too many metals are accreted onto dust grains at $z < 2$ in the [Hou et al. \(2019\)](#) model.

- Notable successes of the models include the good match between DTG and DTM predicted by the [Graziani et al. \(2020\)](#) model at $z > 4$ and observations, the agreement between observations of the DTG and DTM for galaxies at $z > 2$ with the predictions by [Vijayan et al. \(2019\)](#) and [Hou et al. \(2019\)](#) models and that the [Popping et al. \(2017\)](#) and [Li et al. \(2019\)](#) models reproduce at all redshifts the DTG of galaxies with metallicities larger than $12 + \log(O/H) = 8$.

- Using the derived relation between DTG and metallicity, the cold gas mass of galaxies can be more reliably estimated from their millimeter dust-continuum brightness or dust mass, taking metallicity dependencies into account.

The comparison of the observational and theoretical compilations

of the DTG and DTM properties of galaxies demonstrates the power of dust-physics in constraining galaxy formation models. These results will be ever more constraining once the grain properties of dust (size distribution and composition) are better characterised through future optical and space- and ground-based NIR studies (e.g., from the James Webb Space Telescope and Extremely Large Telescope). A better understanding of the buildup of dust and their properties will have tremendous implications for galaxy formation and evolution as a whole, ranging from better constraining the timescales of star-formation as well as the buildup of dust in the ISM to shield UV radiation, to the effect that various types of dust grains have on the absorption and re-emission of stellar radiation.

ACKNOWLEDGEMENTS

The authors thank Luca Graziani, Kuan-Chou Hou, Qi Li, Dian Triani and Aswin Vijayan for making available to us model predictions, providing insights into the workings of the models and providing comments on an earlier version of this paper. The authors also thank Ryan McKinnon, Mark Vogelsberger and Xuejian Shen for useful discussions regarding the [McKinnon et al. \(2018\)](#) model. This work initiated from a discussion with Alice Shapley and benefited from discussions with Felix Priestley, Desika Narayanan and Michele Ginolfi. The authors furthermore thank the anonymous referee for a constructive report.

DATA AVAILABILITY

The compilations of observations and model predictions that support the findings of this study are available on request from the corresponding author.

REFERENCES

- Aoyama S., Hou K.-C., Shimizu I., Hirashita H., Todoroki K., Choi J.-H., Nagamine K., 2017, *MNRAS*, **466**, 105
- Asano R. S., Takeuchi T. T., Hirashita H., Inoue A. K., 2013, *Earth, Planets and Space*, **65**, 213
- Augustin R., et al., 2018, *MNRAS*, **478**, 3120
- Berg T. A. M., et al., 2021, *MNRAS*, **502**, 4009
- Bertemes C., et al., 2018, *MNRAS*, **478**, 1442
- Bianchi S., Schneider R., 2007, *MNRAS*, **378**, 973
- Blitz L., 1993, in Levy E. H., Lunine J. I., eds, *Protostars and Planets III*. p. 125
- Blitz L., Rosolowsky E., 2006, *ApJ*, **650**, 933
- Bocchio M., Marassi S., Schneider R., Bianchi S., Limongi M., Chieffi A., 2016, *A&A*, **587**, A157
- Bouwens R., et al., 2020, *ApJ*, **902**, 112
- Buat V., Boselli A., Gavazzi G., Bonfanti C., 2002, *A&A*, **383**, 801
- Calzetti D., Armus L., Bohlin R. C., Kinney A. L., Koornneef J., Storchi-Bergmann T., 2000, *ApJ*, **533**, 682
- Cazaux S., Spaans M., 2009, *A&A*, **496**, 365
- Ceccarelli C., Viti S., Balucani N., Taquet V., 2018, *MNRAS*, **476**, 1371
- Chabrier G., 2003, *Publications of the Astronomical Society of the Pacific*, **115**, 763
- Chiang I.-D., Sandstrom K. M., Chasteney J., Johnson L. C., Leroy A. K., Utomo D., 2018, *ApJ*, **865**, 117
- Chon S., Omukai K., Schneider R., 2021, *MNRAS*, **508**, 4175
- Croton D. J., et al., 2016, *ApJS*, **222**, 22
- Davé R., Anglés-Alcázar D., Narayanan D., Li Q., Rafieferantsoa M. H., Appleby S., 2019, *MNRAS*, **486**, 2827
- De Cia A., 2018, *A&A*, **613**, L2
- De Cia A., Ledoux C., Savaglio S., Schady P., Vreeswijk P. M., 2013, *A&A*, **560**, A88
- De Cia A., Ledoux C., Mattsson L., Petitjean P., Srianand R., Gavignaud I., Jenkins E. B., 2016, *A&A*, **596**, A97
- De Cia A., Ledoux C., Petitjean P., Savaglio S., 2018, *A&A*, **611**, A76
- De Vis P., et al., 2019, *A&A*, **623**, A5
- Draine B. T., 1978, *ApJS*, **36**, 595
- Draine B. T., 2003, *Annual Review of Astronomy and Astrophysics*, **41**, 241
- Draine B. T., Li A., 2007, *ApJ*, **657**, 810
- Dutta R., et al., 2021, *MNRAS*, **508**, 4573
- Dwek E., 1998, *ApJ*, **501**, 643
- Dwek E., 2016, *ApJ*, **825**, 136
- Dwek E., Scalo J. M., 1980, *ApJ*, **239**, 193
- Feldmann R., 2015, *MNRAS*, **449**, 3274
- Ferrara A., Peroux C., 2021, *MNRAS*, **503**, 4537
- Ferrara A., Viti S., Ceccarelli C., 2016, *MNRAS*, **463**, L112
- Ferrarotti A. S., Gail H. P., 2006, *A&A*, **447**, 553
- Fu J., Kauffmann G., Li C., Guo Q., 2012, *MNRAS*, **424**, 2701
- Fudamoto Y., et al., 2021, *Nature*, **597**, 489
- Fukui Y., Kawamura A., 2010, *ARA&A*, **48**, 547
- Galamez M., Madden S. C., Galliano F., Hony S., Bendo G. J., Sauvage M., 2011, *A&A*, **532**, A56
- Galliano F., Dwek E., Charnal P., 2008, *ApJ*, **672**, 214
- Galliano F., et al., 2021, *A&A*, **649**, A18
- Giannetti A., et al., 2017, *A&A*, **606**, L12
- Ginolfi M., Graziani L., Schneider R., Marassi S., Valiante R., Dell’Aglì F., Ventura P., Hunt L. K., 2018, *MNRAS*, **473**, 4538
- Glatzle M., Graziani L., Ciardi B., 2022, *MNRAS*, **510**, 1068
- Gnedin N. Y., 2010, *ApJ*, **721**, L79
- Goldsmith P. F., 2001, *ApJ*, **557**, 736
- Gong M., Ostriker E. C., Wolfire M. G., 2017, *ApJ*, **843**, 38
- Gould R. J., Salpeter E. E., 1963, *ApJ*, **138**, 393
- Graziani L., Schneider R., Ginolfi M., Hunt L. K., Maio U., Glatzle M., Ciardi B., 2020, *MNRAS*, **494**, 1071
- Gruppioni C., et al., 2020, *A&A*, **643**, A8
- Hamanowicz A., Peroux C., Zwaan M. A., Rahmani H. e. a., 2020, *MNRAS*, Submitted
- Henriques B. M. B., White S. D. M., Thomas P. A., Angulo R., Guo Q., Lemson G., Springel V., Overzier R., 2015, *MNRAS*, **451**, 2663
- Hirashita H., Kuo T.-M., 2011, *MNRAS*, **416**, 1340
- Hirashita H., Tajiri Y. Y., Kamaya H., 2002, *A&A*, **388**, 439
- Hollenbach D., Salpeter E. E., 1971, *ApJ*, **163**, 155
- Hollenbach D., Kaufman M. J., Neufeld D., Wolfire M., Goicoechea J. R., 2012, *ApJ*, **754**, 105
- Hopkins P. F., 2015, *MNRAS*, **450**, 53
- Hou K.-C., Hirashita H., Nagamine K., Aoyama S., Shimizu I., 2017, *MNRAS*, **469**, 870
- Hou K.-C., Aoyama S., Hirashita H., Nagamine K., Shimizu I., 2019, *MNRAS*, **485**, 1727
- Hu W., et al., 2019, *MNRAS*, **489**, 1619
- Ishiki S., Okamoto T., 2017, *MNRAS*, **466**, L123
- Issa M. R., MacLaren I., Wolfendale A. W., 1990, *A&A*, **236**, 237
- Ivlev A. V., Padovani M., Galli D., Caselli P., 2015, *ApJ*, **812**, 135
- Jenkins E. B., 2009, *ApJ*, **700**, 1299
- Jenkins E. B., Wallerstein G., 2017, *ApJ*, **838**, 85
- Kaasinen M., et al., 2019, *ApJ*, **880**, 15
- Kannan R., Garaldi E., Smith A., Pakmor R., Springel V., Vogelsberger M., Hernquist L., 2021, arXiv e-prints, p. arXiv:2110.00584
- Kataoka A., Okuzumi S., Tanaka H., Nomura H., 2014, *A&A*, **568**, A42
- Kennicutt R. C., Evans N. J., 2012, *ARA&A*, **50**, 531
- Kewley L. J., Ellison S. L., 2008, *ApJ*, **681**, 1183
- Kewley L. J., Nicholls D. C., Sutherland R. S., 2019, *ARA&A*, **57**, 511
- Krumholz M. R., Leroy A. K., McKee C. F., 2011, *ApJ*, **731**, 25
- Lagos C. D. P., Baugh C. M., Lacey C. G., Benson A. J., Kim H.-S., Power C., 2011, *MNRAS*, **418**, 1649
- Larson R. B., 2005, *MNRAS*, **359**, 211
- Li Q., Narayanan D., Davé R., 2019, *MNRAS*, **490**, 1425

- Li Q., Narayanan D., Torrey P., Davé R., Vogelsberger M., 2020, arXiv e-prints, p. [arXiv:2012.03978](https://arxiv.org/abs/2012.03978)
- Liang L., et al., 2019, *MNRAS*, **489**, 1397
- Lianou S., Barmby P., Mosenkov A., Lehnert M., Karczewski O., 2019, arXiv e-prints, p. [arXiv:1906.02712](https://arxiv.org/abs/1906.02712)
- Lisenfeld U., Ferrara A., 1998, *ApJ*, **496**, 145
- Madau P., Dickinson M., 2014, *ARA&A*, **52**, 415
- Maio U., Ciardi B., Yoshida N., Dolag K., Tornatore L., 2009, *A&A*, **503**, 25
- Maiolino R., Mannucci F., 2019, *A&ARv*, **27**, 3
- Mancini M., Schneider R., Graziani L., Valiante R., Dayal P., Maio U., Ciardi B., Hunt L. K., 2015, *MNRAS*, **451**, L70
- Martínez-González S., Wunsch R., Silich S., Tenorio-Tagle G., Palouš J., Ferrara A., 2019, *ApJ*, **887**, 198
- Mattsson L., Wahlin R., Höfner S., 2010, *A&A*, **509**, A14
- Mattsson L., De Cia A., Andersen A. C., Petitjean P., 2019, *A&A*, **624**, A103
- McKee C., 1989, in Allamandola L. J., Tielens A. G. G. M., eds, Vol. 135, *Interstellar Dust*. p. 431
- McKee C. F., Krumholz M. R., 2010, *ApJ*, **709**, 308
- McKinnon R., Vogelsberger M., Torrey P., Marinacci F., Kannan R., 2018, *MNRAS*, **478**, 2851
- Ménard B., Scranton R., Fukugita M., Richards G., 2010, *MNRAS*, **405**, 1025
- Naab T., Ostriker J. P., 2017, *ARA&A*, **55**, 59
- Nozawa T., Kozasa T., Habe A., 2006, *ApJ*, **648**, 435
- Okuzumi S., Tanaka H., Sakagami M.-a., 2009, *ApJ*, **707**, 1247
- Omukai K., 2000, *ApJ*, **534**, 809
- Omukai K., Tsuribe T., Schneider R., Ferrara A., 2005, *ApJ*, **626**, 627
- Ostriker J., Silk J., 1973, *ApJ*, **184**, L113
- Peek J. E. G., Ménard B., Corrales L., 2015, *ApJ*, **813**, 7
- Peeples M. S., Werk J. K., Tumlinson J., Oppenheimer B. D., Prochaska J. X., Katz N., Weinberg D. H., 2014, *ApJ*, **786**, 54
- Péroux C., Howk J. C., 2020, *ARA&A*, **58**, 363
- Péroux C., Petitjean P., Aracil B., Srianand R., 2002, *New Astron.*, **7**, 577
- Péroux C., Dessauges-Zavadsky M., D’Odorico S., Kim T.-S., McMahon R. G., 2007, *MNRAS*, **382**, 177
- Péroux C., et al., 2019, *MNRAS*, **485**, 1595
- Péroux C., Nelson D., van de Voort F., Pillepich A., Marinacci F., Vogelsberger M., Hernquist L., 2020, *MNRAS*, **499**, 2462
- Pilyugin L. S., Grebel E. K., 2016, *MNRAS*, **457**, 3678
- Popping G., Somerville R. S., Trager S. C., 2014, *MNRAS*, **442**, 2398
- Popping G., Behroozi P. S., Peeples M. S., 2015, *MNRAS*, **449**, 477
- Popping G., Somerville R. S., Galametz M., 2017, *MNRAS*, **471**, 3152
- Poudel A., Heinämäki P., Tempel E., Einasto M., Lietzen H., Nurmi P., 2017, *A&A*, **597**, A86
- Quiét S., et al., 2016, *MNRAS*, **458**, 4074
- Rahmani H., et al., 2016, *MNRAS*, **463**, 980
- Rémy-Ruyer A., et al., 2014, *A&A*, **563**, A31
- Roman-Duval J., et al., 2014, *ApJ*, **797**, 86
- Roman-Duval J., et al., 2019, *ApJ*, **871**, 151
- Roman-Duval J., et al., 2021, *ApJ*, **910**, 95
- Roman-Duval J., et al., 2022, arXiv e-prints, p. [arXiv:2202.04765](https://arxiv.org/abs/2202.04765)
- Romano L. E. C., Nagamine K., Hirashita H., 2022, arXiv e-prints, p. [arXiv:2202.05521](https://arxiv.org/abs/2202.05521)
- Salim S., Narayanan D., 2020, *ARA&A*, **58**, 529
- Schneider R., Ferrara A., Salvaterra R., 2004, *MNRAS*, **351**, 1379
- Schneider R., Omukai K., Inoue A. K., Ferrara A., 2006, *MNRAS*, **369**, 1437
- Scoville N., et al., 2017, *ApJ*, **837**, 150
- Scudder J. M., Ellison S. L., El Meddah El Idrissi L., Poetrodjojo H., 2021, *MNRAS*, **507**, 2468
- Shapley A. E., Cullen F., Dunlop J. S., McLure R. J., Kriek M., Reddy N. A., Sanders R. L., 2020, *ApJ*, **903**, L16
- Somerville R. S., Primack J. R., 1999, *MNRAS*, **310**, 1087
- Somerville R. S., Hopkins P. F., Cox T. J., Robertson B. E., Hernquist L., 2008, *MNRAS*, **391**, 481
- Somerville R. S., Popping G., Trager S. C., 2015, *MNRAS*, **453**, 4337
- Sparre M., et al., 2014, *ApJ*, **785**, 150
- Springel V., Di Matteo T., Hernquist L., 2005a, *MNRAS*, **361**, 776
- Springel V., et al., 2005b, *Nature*, **435**, 629
- Steidel C. C., Adelberger K. L., Giavalisco M., Dickinson M., Pettini M., 1999, *ApJ*, **519**, 1
- Takeuchi T. T., Buat V., Heinis S., Giovannoli E., Yuan F. T., Iglesias-Páramo J., Murata K. L., Burgarella D., 2010, *A&A*, **514**, A4
- Temim T., Dwek E., Tchernyshyov K., Boyer M. L., Meixner M., Gall C., Roman-Duval J., 2015, *ApJ*, **799**, 158
- Tornatore L., Ferrara A., Schneider R., 2007a, *MNRAS*, **382**, 945
- Tornatore L., Borgani S., Dolag K., Matteucci F., 2007b, *MNRAS*, **382**, 1050
- Triani D. P., Sinha M., Croton D. J., Pacifici C., Dwek E., 2020, *MNRAS*, **493**, 2490
- Vijayan A. P., Clay S. J., Thomas P. A., Yates R. M., Wilkins S. M., Henriques B. M., 2019, *MNRAS*, **489**, 4072
- Vílchez J. M., Relaño M., Kennicutt R., De Looze I., Mollá M., Galametz M., 2019, *MNRAS*, **483**, 4968
- Vladilo G., 2004, *A&A*, **421**, 479
- Vogelsberger M., McKinnon R., O’Neil S., Marinacci F., Torrey P., Kannan R., 2019, *MNRAS*, **487**, 4870
- Walter F., et al., 2020, *ApJ*, **902**, 111
- Wang T.-M., et al., 2022, arXiv e-prints, p. [arXiv:2201.12070](https://arxiv.org/abs/2201.12070)
- Wendt M., Bouché N. F., Zabl J., Schroetter I., Muzahid S., 2021, *MNRAS*, **502**, 3733
- Whitworth A., Boffin H., Watkins S., Francis N., 1998, *Astronomy and Geophysics*, **39**, 10
- Wiseman P., Schady P., Bolmer J., Krühler T., Yates R. M., Greiner J., Fynbo J. P. U., 2017, *A&A*, **599**, A24
- Yamasawa D., Habe A., Kozasa T., Nozawa T., Hirashita H., Umeda H., Nomoto K., 2011, *ApJ*, **735**, 44
- Zafar T., Popping A., Péroux C., 2013, *A&A*, **556**, 140
- Zhukovska S., 2014, *A&A*, **562**, A76
- Zhukovska S., Gail H. P., Tieloff M., 2008, *A&A*, **479**, 453
- de Bannassuti M., Schneider R., Valiante R., Salvadori S., 2014, *MNRAS*, **445**, 3039